Dalton Transactions

An international journal of inorganic chemistry

www.rsc.org/dalton

Number 43 | 21 November 2007 | Pages 4873–5092

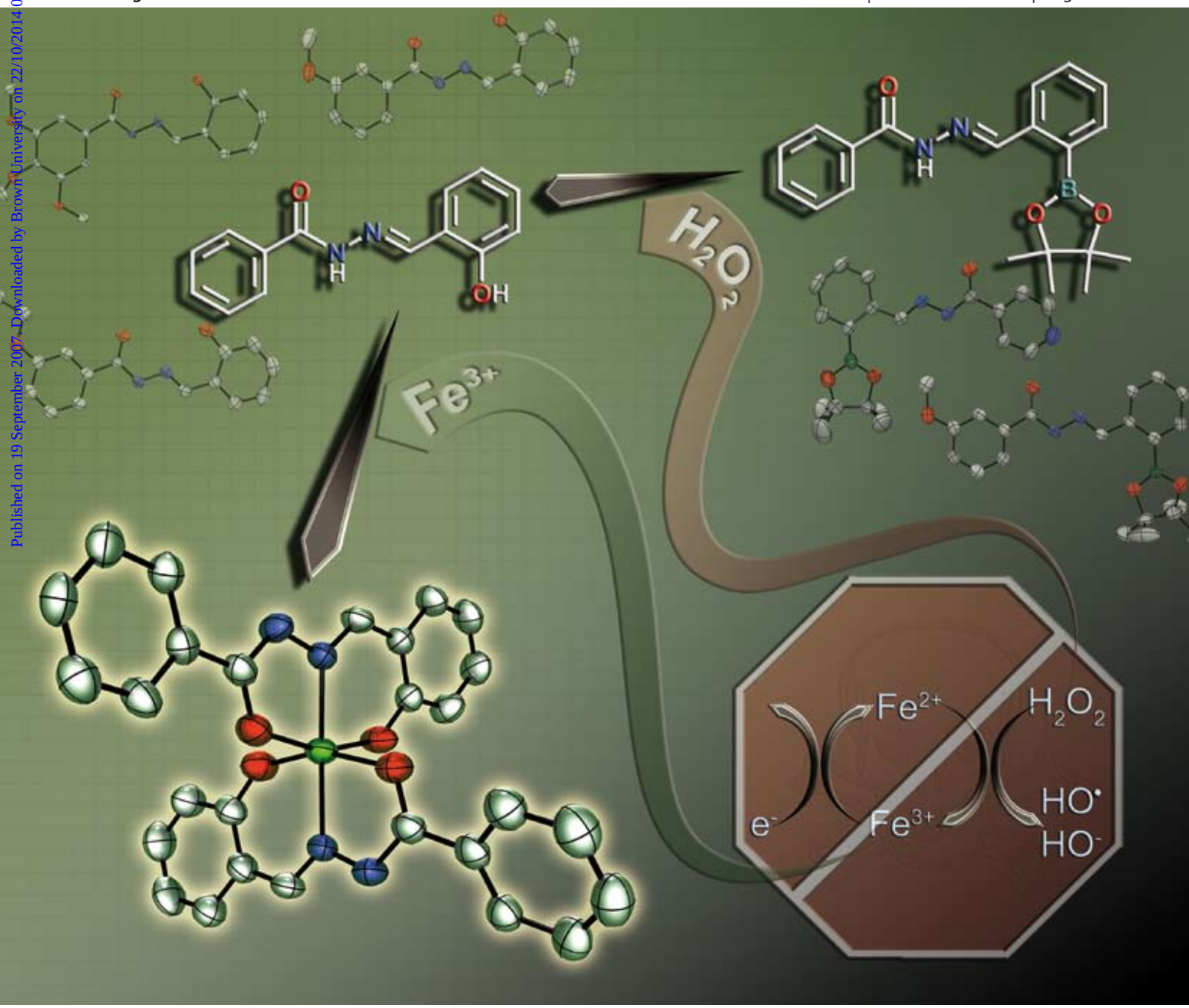

ISSN 1477-9226

HOT ARTICLE
Katherine J. Franz *et al.*
Modifications of boronic ester pro-chelators triggered by hydrogen peroxide tune reactivity to inhibit metal-promoted oxidative stress

HOT ARTICLE
Philip J. Blower and Stephen J. Mather *et al.*
How do HYNIC-conjugated peptides bind technetium? Insights from LC-MS and stability studies

RSC Publishing

Modifications of boronic ester pro-chelators triggered by hydrogen peroxide tune reactivity to inhibit metal-promoted oxidative stress‡†§

Louise K. Charkoudian, David M. Pham, Ashley M. Kwon, Abbey D. Vangeloff and Katherine J. Franz*

Received 5th April 2007, Accepted 19th June 2007
First published as an Advance Article on the web 19th September 2007
DOI: 10.1039/b705199a

Several new analogs of salicylaldehyde isonicotinoyl hydrazone (SIH) and salicylaldehyde benzoyl hydrazone (SBH) that contain an aryl boronic ester (BSIH, BSBH) or acid (BASIH) in place of an aryl hydroxide have been synthesized and characterized as masked metal ion chelators. These pro-chelators show negligible interaction with iron(III), although the boronic acid versions exhibit some interaction with copper(II), zinc(II) and nickel(II). Hydrogen peroxide oxidizes the aryl boronate to phenol, thus converting the pro-chelators to tridentate ligands with high affinity metal binding properties. An X-ray crystal structure of a bis-ligated iron(III) complex, $[Fe(SBH(m\text{-}OMe)_3)_2]NO_3$, confirms the meridonal binding mode of these ligands. Modifications of the aroyl ring of the chelators tune their iron affinity, whereas modifications on the boron-containing ring of the pro-chelators attenuate their reaction rates with hydrogen peroxide. Thus, the methoxy derivative pro-chelator (*p*-OMe)BASIH reacts with hydrogen peroxide nearly 5 times faster than the chloro derivative (*m*-Cl)BASIH. Both the rate of pro-chelator to chelator conversion as well as the metal binding affinity of the chelator influence the overall ability of these molecules to inhibit hydroxyl radical formation catalyzed by iron or copper in the presence of hydrogen peroxide and ascorbic acid. This pro-chelator strategy has the potential to improve the efficacy of medicinal chelators for inhibiting metal-promoted oxidative stress.

Introduction

Oxidative stress is implicated in a wide variety of diseases, including but not limited to diabetes, atherosclerosis, aging, macular degeneration, and neurodegeneration.[1–4] Depending on properties of their coordination environment, metal ions like copper and iron can catalyze the production of highly reactive hydroxyl radicals ($OH^{\bullet}$)[5] that damage lipids, proteins and nucleic acids. Metal-promoted oxidative stress may therefore be a critical component in diseases where normal metal ion homeostasis is impaired or where aberrant metal accumulation occurs.[6] For example, the iron load in the *substantia nigra* brain region of Parkinson's disease patients is 35% higher than that in healthy age-matched controls,[7,8] and iron levels in maculas of those 65 or older are higher than those under 65.[9] Inhibiting iron-promoted oxidative stress by inactivating catalytic iron is therefore a promising strategy for treating such diseases.[10–17]

While chelating agents developed for iron-overload diseases have been proposed for use in degenerative diseases, their intrinsic affinity for other essential metals like zinc and copper may have toxic consequences. In addition, their high affinity for iron results in competition with essential iron-containing enzymes. For example, treatment of macular degeneration with desferrioxamine is associated with retinal toxicity hypothesized to result from overall retinal iron deficiency.[9]

Our strategy to develop targeted iron chelators is to synthesize "masked" chelators that have little to no affinity for metal ions until the mask is selectively removed by the presence of reactive oxygen species such as hydrogen peroxide (H_2O_2). The goal is to develop reagents that are activated only under disease conditions to reveal high-affinity iron-binding ligands that compete for the redox-active iron that is the source of $OH^{\bullet}$ generation. Our first-generation pro-chelator, BSIH,[18] contains a boronic ester in place of a phenolic oxygen that is a key donor atom of salicylaldehyde isonicotinoyl hydrazone (SIH), a well-studied high-affinity, membrane permeable ligand that scavenges and incapacitates redox-active iron.[19–21] Aryl boronic acids and their esters are well known to deboronate *via* oxidation of the carbon–boron bond initiated by nucleophilic attack by H_2O_2, followed by aryl migration to a borate intermediate that rapidly hydrolyzes to give the phenol and borate ester or boric acid.[22] This reactivity has made boronic esters attractive targets for the development of highly selective fluorescent probes for H_2O_2.[23–27] Boronic acids do not appear to have intrinsic toxicity issues, and the end product boric acid is considered non-toxic to humans.[28] These properties coupled with their relative stability make them useful for a variety of biological and medicinal applications.[28]

As shown in Scheme 1, H_2O_2 reacts selectively to convert BSIH to SIH, which forms a stable bis-ligated complex with Fe^{3+}. In this report, we present the synthesis, characterization, and hydroxyl radical inhibition capacities of six additional BSIH analogs together with their unmasked chelator versions and iron complexes. By varying the substituents on these analogs, several properties of the pro-chelator/chelator combinations can be tuned, including lipophilicity, iron binding affinity, and

Department of Chemistry, Duke University, Durham, NC, 27708–0346, USA. E-mail: katherine.franz@duke.edu; Fax: +1 919 660 1605; Tel: +1 919 660 1541

† Based on the presentation given at Dalton Discussion No. 10, 3rd–5th September 2007, University of Durham, Durham, UK.

‡ CCDC reference numbers 643169–643174. For crystallographic data in CIF or other electronic format see DOI: 10.1039/b705199a

§ Electronic supplementary information (ESI) available: Crystallographic details, including full atom-numbering schemes, and NMR spectra. See DOI: 10.1039/b705199a

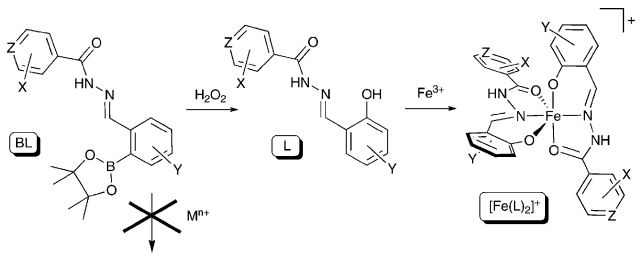

Scheme 1 Boronate-masked aroyl hydrazone pro-chelators "BL" are weak metal-binding ligands, but are converted by H_2O_2 to chelators "L" that bind Fe^{3+} to form bis-ligated $[FeL_2]^+$ complexes. X and Y are chloro, methoxy, or ethoxy substituents, while Z is either N or CH.

rate of H_2O_2-dependent unmasking of the pro-chelator to the chelator.

Results and discussion

Synthesis, nomenclature and structure of pro-chelators and chelators

The compounds shown in Fig. 1 were synthesized by a straightforward Schiff base condensation reaction between aryl hydrazides and aryl aldehydes in acidic aqueous or methanolic solution. This class of aroyl hydrazone compounds has shown wide utility as tridentate metal chelating agents.[29] The pro-chelators presented here are based on two families of aroyl hydrazone ligands, those of salicylaldehyde isonicotinoyl hydrazone (SIH) and salicylaldehyde benzoyl hydrazone (SBH). Our first generation pro-chelator replaced the phenol of SIH with a boronic acid pinacol ester and was given the abbreviation BSIH.[18] Derivatives in which a boronic acid moiety replaces the boronic ester are denoted BASIH. Substitution on the B- or OH-containing ring is designated by the substituent in parentheses before the abbreviation. For example, the pro-chelators (*p*-OMe)BASIH and (*m*-Cl)BASIH and their corresponding chelators (*p*-OMe)SIH and (*m*-Cl)SIH in Fig. 1a. Derivatives with substituents on the aroyl ring are based on the SBH ligand and are designated with the substituent in parentheses after the abbreviation. These compounds include the pro-chelators BSBH(*m*-OMe), BSBH(*m*-OEt) and BSBH(OMe)$_3$ and their corresponding chelators SBH(*m*-OMe), SBH(*m*-OEt) and SBH(OMe)$_3$, all shown in Fig. 1b. Finally, benzaldehyde isonicotinoyl hydrazone (BIH) was also prepared as a control compound that contains the hydrazone functionality but lacks the key metal-binding phenol group (Fig. 1c).

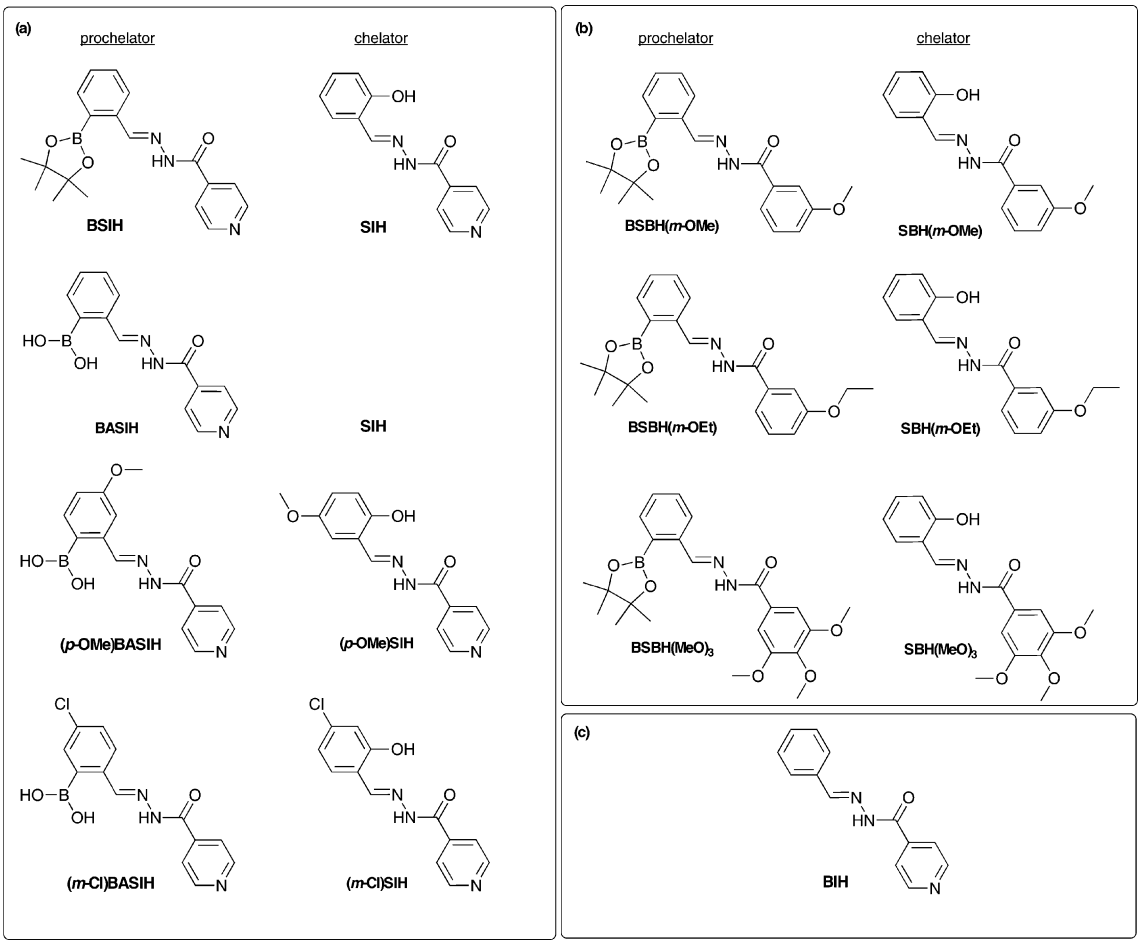

Fig. 1 Chemical structures and abbreviations of the pro-chelators (left-hand columns) and chelators (right-hand columns) used in this study. (a) Derivatives of salicylaldehyde isonicotinoyl hydrazone (SIH) and their boronic ester (BSIH) or boronic acid (BASIH) prochelators with modifications on the B/OH-containing ring, (b) derivatives of salicylaldehyde benzoyl hydrazone (SBH) and their boronic ester prochelators (BSBH) with modifications on the aroyl ring, (c) benzaldehyde isonicotinoyl hydrazone.

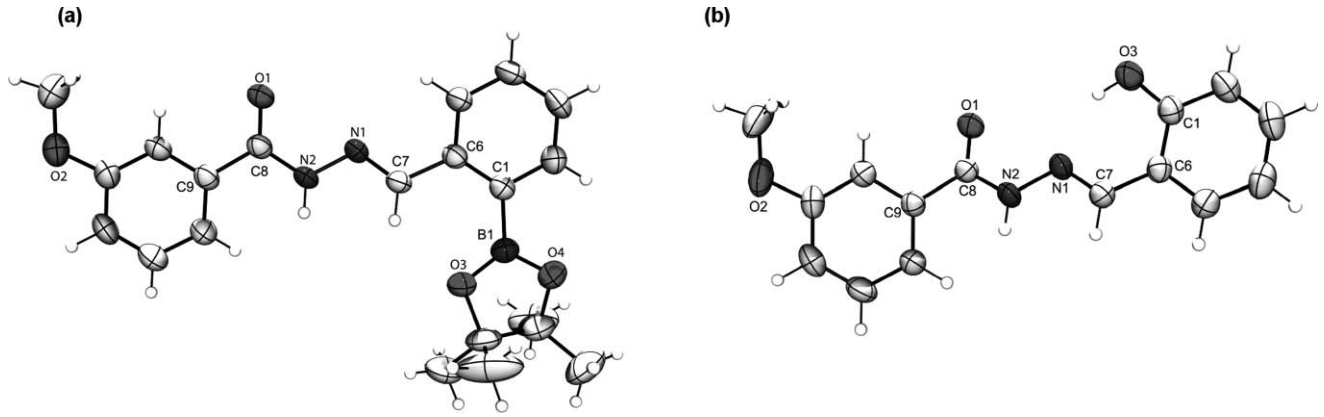

Fig. 2 ORTEP structural diagrams showing 50% probability ellipsoids and partial atom numbering schemes for (a) the pro-chelator BSBH(*m*-OMe) and (b) its chelating version SBH(*m*-OMe).

As with BSIH,[18] the X-ray crystal structures of BSBH(*m*-OMe) and BSBH(*m*-OEt) reveal that in the crystalline solid the B atom in all cases is *anti* to the imine N1 atom and the configuration about the C7=N1 bond is *E*. The *E* configuration is retained in the structures of the corresponding chelators, but the phenolic OH assumes a *syn* conformation. Fig. 2 shows the structures of the BSBH(*m*-OMe) and SBH(*m*-OMe) pro-chelator/chelator pair; a summary of X-ray diffraction parameters is found in Table 1 and selected bond distances and angles are collected in Table 2. The structures of *m*-ethoxy analogs BSBH(*m*-OEt) and SBH(*m*-OEt) as well as the trimethoxy SBH(OMe)$_3$ chelator are found in the ESI.§

The *syn* conformation adopted by the chelators is stabilized by a hydrogen bond between the phenolic hydrogen and the imine nitrogen ($d_{SBH(m\text{-}OMe)} = 2.653(1)$ Å; $d_{SBH(m\text{-}OEt)} = 2.619(1)$ Å; $d_{SBH(OMe)3} = 2.656(3)$ Å). This conformation favorably arranges the carbonyl O, imine N and phenol O on the same face for tridentate metal binding.

As anticipated, the bis-ligated $[FeL_2]^+$ complexes contain a ferric ion in distorted octahedral geometry with two SIH-type ligands bound in meridonal configuration with tridentate coordination. An example is shown in Fig. 3 for the SBH(OMe)$_3$ derivative. Selected bond lengths and angles are in Tables 2 and 3. Although crystals have also been obtained for $[Fe(SIH)_2]^+$ and $[Fe(SBH(m\text{-}OEt))_2]^+$ and preliminary diffraction data reveal similar structural trends, $[Fe(SBH(OMe)_3)_2]^+$ is the only derivative that has provided high-quality data to date.

A Cambridge Structural Database search of aroyl hydrazones returns several derivatized SIH, PIH and SBH analogs (where PIH is pyridoxyl isonicotinoyl hydrazone) along with a diverse number of metal complexes spanning from first row transition metals to uranium. Among this rich array of complexes there are surprisingly few iron examples, and these only include mono-ligated complexes of the type $[FeCl_2(MeOH)(L)]$.[30–32] The structure of $[Fe(SBH(OMe)_3)_2]^+$ in Fig. 3 therefore represents the first structurally characterized example of the bis-ligated form, which is the expected speciation in biological environments of pH 7.4. Table 3 highlights the consistency in the iron coordination geometry and bond lengths between the mono-ligated structures and that of $[Fe(SBH(OMe)_3)_2]NO_3$. The phenolate O–Fe distance is the shortest donor atom-to-Fe distance in all cases, being 1.88 Å in the $[Fe(SBH(OMe)_3)_2]NO_3$ example.

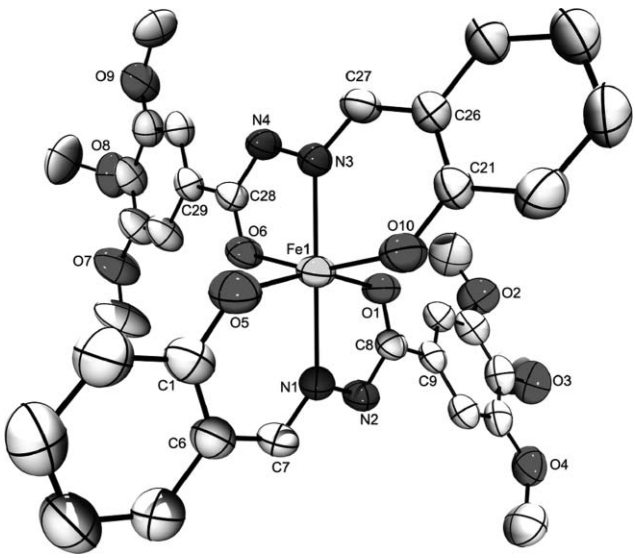

Fig. 3 ORTEP structural diagram showing 50% probability ellipsoids and partial atom numbering scheme for $[Fe(SBH(MeO)_3)_2]^+$. Each SBH ligand coordinates Fe through its phenolate O (O5, O10), imine N (N1, N3), and carbonyl O (O1, O6). The phenolate O is the one masked by B in the pro-chelators. The nitrate counter anion is not shown.

A comparative analysis of 15 derivatives of SIH and SBH metal complexes of the first and second row transition metals shows that the positions of the three donor atoms shift on average only ~0.04 Å across the series. Furthermore, projection of a set of 18 SIH and SBH ligand structures onto the Fe(SBH) coordinates shows that the free ligands need only shift ~0.09 Å to accommodate iron binding (see ESI§). This analysis illustrates that even in the absence of a coordinating metal center, derivatives of SIH and SBH are conformationally pre-arranged with optimized geometry for metal coordination.

Metal specificity

Initial assessment of BSIH and iron suggested that a strong Fe^{3+} complex only forms once the pro-chelator is converted to the SIH chelator.[18] In order to assess the interaction between the pro-chelators and metals in more detail, UV-vis experiments were conducted at concentrations that enable visualization of weak

Table 1 Summary of X-ray diffraction parameters

	$[Fe(SBH(OMe)_3)_2]NO_3 \cdot$ Pentanes	SBH(*m*-OMe)	SBH(*m*-OEt)	$SBH(OMe)_3$	BSBH(*m*-OMe)	$[BSBH(m\text{-}OEt)]_2 \cdot H_2O$
Formula	$C_{39}\ H_{34}\ Fe\ N_5\ O_{13}$	$C_{15}\ H_{14}\ N_2\ O_3$	$C_{16}\ H_{16}\ N_2\ O_3$	$C_{17}\ H_{18}\ N_2\ O_5$	$C_{21}\ H_{25}\ B\ N_2\ O_4$	$C_{44}\ H_{56}\ B_2\ N_4\ O_9$
FW	836.56	270.28	284.31	330.33	380.24	806.55
a/Å	11.7263(11)	11.4645(9)	11.5979(3)	14.787(7)	17.8735(16)	18.293(7)
b/Å	28.622(3)	13.6942(11)	14.0704(3)	13.198(6)	12.7925(10)	8.639(3)
c/Å	12.2079(13)	8.5467(8)	9.4947(3)	8.225(2)	9.0933(9)	29.494(10)
α/°	90	90	90	90	90	90
β/°	96.464(5)	92.025(4)	110.1330(10)	101.262(5)	90	100.504(5)
γ/°	90	90	90	90	90	90
V/Å^3	4071.3(7)	1341.0(2)	1454.74(7)	1574.2(11)	2079.2(3)	4583(3)
Z	4	4	4	4	4	4
Cryst. syst.	Monoclinic	Monoclinic	Monoclinic	Monoclinic	Orthorhombic	Monoclinic
Space group	$P\ 2_1/c$	$P\ 2_1/c$	$P\ 2_1/c$	$P\ 2_1/c$	$P\ c\ a\ 2_1$	$P\ 2_1/n$
T/K	298(2)	173(2)	298(2)	173(2)	298(2)	298(2)
λ/Å	0.71073	0.71073	0.71073	0.71073	0.71073	0.71073
ρ/g cm^{-3}	1.365	1.339	1.298	1.394	1.215	1.179
μ/mm^{-1}	0.44	0.095	0.091	0.104	0.083	0.081
R_1 (obsd data)	0.731	0.0415	0.0392	0.05	0.0427	0.0828
wR_2 (all data, $F2$ refinement)	0.2733	0.1122	0.1081	0.1092	0.1185	0.2631

Table 2 Selected bond lengths and bond angles of chelators, prochelators, and $[Fe(SBH(OMe)_3)_2]NO_3$

	$[Fe(SBH(OMe)_3)_2]$ $NO_3 \cdot$Pentanes[a]	SBH(*m*-OMe)[b]	SBH(*m*-OEt)[b]	$SBH(OMe)_3$[a]	BSBH(*m*-OMe)[c]	$[BSBH(m\text{-}OEt)]_2 \cdot H_2O$[c]
Bond lengths/Å						
O1–C8	1.266(5)	1.231(1)	1.224(1)	1.238(3)	1.231(3)	1.237(4)
C1–X	1.312(5)	1.354(2)	1.353(2)	1.349(3)	1.557(4)	1.562(6)
N1–N2	1.376(5)	1.383(1)	1.374(1)	1.375(3)	1.381(2)	1.375(4)
N1–C7	1.281(6)	1.276(2)	1.271(2)	1.277(3)	1.272(3)	1.273(5)
N2–C8	1.325(5)	1.339(2)	1.352(2)	1.334(3)	1.358(3)	1.357(5)
Bond angles/°						
O1–C8–C9	122.3(4)	121.6(1)	121.7(1)	122.5(2)	121.3(2)	121.0(3)
O1–C8–N2	119.0(4)	123.1(1)	122.2(1)	123.2(2)	122.4(2)	122.0(3)
N2–C8–C9	118.7(4)	115.3(1)	116.1(1)	114.3(2)	116.4(2)	117.0(3)
N1–N2–C8	116.4(3)	120.2(1)	119.0(1)	121.5(2)	118.7(2)	118.9(3)
N2–N1–C7	118.3(3)	115.5(1)	118.4(1)	114.2(2)	115.8(2)	115.5(3)
N1–C7–C6	124.3(4)	121.7(1)	121.2(1)	122.9(2)	119.1(2)	118.7(3)
C1–C6–C7	122.9(4)	122.8(1)	121.9(1)	122.5(2)	117.2(2)	121.9(3)
C6–C1–X	122.1(5)	121.8(1)	122.0(1)	122.0(2)	126.9(2)	125.8(3)

[a] X = O5. [b] X = O3. [c] X = B1.

complexes with Cu^{2+}, Zn^{2+}, Ni^{2+} and Fe^{3+}. Studies were performed in methanol to ensure solubility of metal salts and chelators.

Fig. 4 shows the visible spectrum between 500–800 nm of a methanolic solution containing 10 mM $Fe(NO_3)_3$ and 10 mM L, where L is one of the pro-chelators BASIH or BSIH, their corresponding chelator SIH, or the potentially bidentate hydrazone BIH. In the absence of metal, none of the L compounds has an absorbance feature in this wavelength range, and $Fe(NO_3)_3$ displays only a weak tail from a band centered around 360 nm. Solutions containing Fe^{3+} and SIH are a deep red color and exhibit a broad d–d absorbance band in this region. In contrast, addition of BIH to $Fe(NO_3)_3$ results in only a very subtle color change from yellow to pale orange, with a feature around 530 nm. Replacing BIH by either BASIH or BSIH results in a slightly more intense orange color and an increase in the shoulder around 530 nm. The spectra of the BASIH and BSIH solutions are nearly indistinguishable, suggesting a similar mode of interaction of the boronic acid and the boronic ester versions of the pro-chelators with Fe^{3+}. They are distinct from the control BIH, however, suggesting that the boron-containing moiety may weakly interact with the metal in addition to the O/N hydrazone feature that all of these compounds share. The pyridine N on the aroyl ring can also interact with metal ions in all of these cases.

When the 10 mM solutions are diluted to 100 μM, the features described above for BSIH, BASIH and BIH are barely perceptible. Furthermore, the pale orange color of the 10 mM solutions disappears when phosphate buffer is added to the methanol solutions, suggesting that phosphate is sufficient for competing Fe^{3+} from these compounds. In contrast, the SIH complex remains intact in phosphate buffer. This analysis suggests that the pro-chelators are unlikely to compete in a biological setting for iron binding until they are unmasked to reveal the chelating version.

Table 3 Comparison of selected bond lengths and bond angles for iron complexes

	$[FeCl_2(S)L]$			$[FeL^4_2]NO_3$	
	L^1	L^2	L^3	*Ligand 1*	*Ligand 2*
Bond lengths/Å					
O–Fe (C=O)	2.068(2)	2.033(3)	2.012(6)	2.091(3)	2.071(3)
N–Fe	2.119(2)	2.135(4)	2.131(6)	2.116(3)	2.091(3)
O–Fe (PhO^-)	1.874(2)	1.897(3)	1.905(6)	1.887(4)	1.884(3)
Bond angles/°					
(C=O) O–Fe–N	74.4(1)	74.3(1)	75.5(2)	74.8(1)	74.7(1)
O–Fe–O	159.3(1)	158.2(1)	159.8(2)	159.4(1)	159.6(1)
N–Fe–O (PhO^-)	85.5(1)	84.8(1)	84.3(2)	84.7(1)	85.1(1)
N1–Fe–N3				167.1(1)	
O1–Fe–O6				89.1(1)	
O5–Fe1–O10				97.0(2)	
O1–Fe1–O10				90.2(1)	
O5–Fe1–O6				90.6(1)	

L^1 = SBH (ref. 30); L^2 = (*p*-MeO)SBH(*m*-OMe) (ref. 31); L^3 = PIH (ref. 32); L^4 = $SBH(OMe_3)$ (*this work*); S = MeOH for L^1 and L^2 and H_2O for L^3.

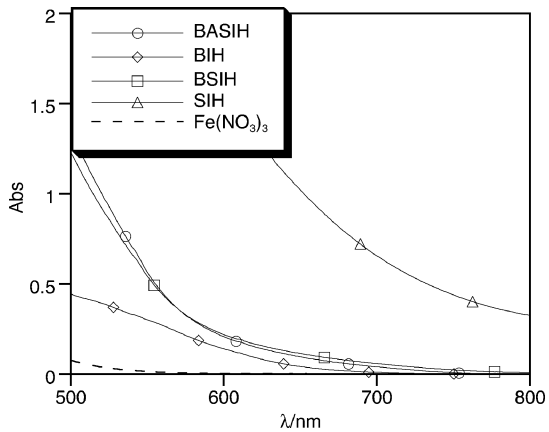

Fig. 4 Visible spectra of 10 mM methanol solutions of Fe^{3+} with 10 mM added BASIH, BIH, BSIH, or SIH. Only SIH forms intensely colored solutions with Fe^{3+}.

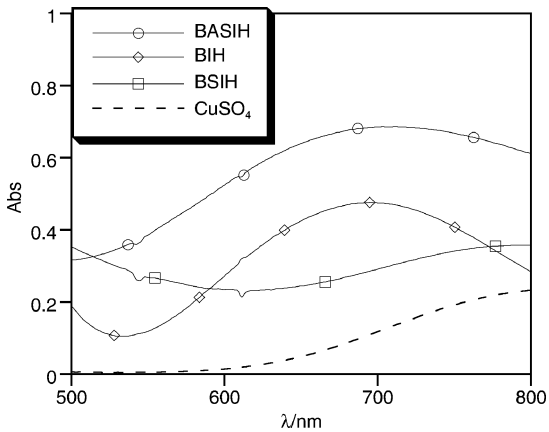

Fig. 5 Visible spectra of 10 mM methanol solutions of $CuSO_4$ with 10 mM added BASIH, BIH, or BSIH. The d–d band of Cu^{2+} centered around 800 nm is most affected by the addition of BIH and BASIH.

In contrast to the very weak interaction with Fe^{3+}, BIH does form a complex with Cu^{2+}, as evidenced by precipitate formation upon addition of BIH to a methanolic solution of $CuSO_4$ and a corresponding color change from very pale blue–green to more intense green. The spectra in Fig. 5 show the shift of the Cu^{2+} d–d band from 800 nm for $CuSO_4$ to 700 nm for the mixture with BIH, clearly indicating a change in coordination environment around Cu^{2+}. The carbonyl O and the imine N of hydrazones are known to form bidentate complexes with Cu^{2+}.[33] When BIH is replaced by BSIH, there is less of a color change and less precipitate formation, although the solution does become cloudy, suggesting some complexation. In the case of Cu^{2+}, the spectra with BSIH and BASIH are distinct. As shown in Fig. 5, the d–d band for the Cu^{2+} plus BASIH solution is more similar to that of the BIH solution than the BSIH solution. Not as much precipitate forms, however, and solutions of Cu^{2+} and BASIH in methanol are a bright aquamarine color as opposed to the green of the BIH complex. As seen in the Fe^{3+} case, mixtures of Cu^{2+} with SIH display the most intense colors among this series. The spectrum is not shown in Fig. 5 since the complex completely precipitates from solution. Complexes of SBH-type ligands with Cu^{2+} are known.[34,35]

Collectively, these results suggest that the N/O unit and/or the pyridine N of these aroyl hydrazones indeed complex Cu^{2+}, and that the boronic acid and boronic ester moieties also participate in these interactions, but to different extents. It appears from these studies that the boronic acid version interacts more strongly than the ester version. Studies with Ni^{2+} and Zn^{2+} support the observation that boronic acid versions of the pro-chelators are more prone to metal interactions than the boronic ester counterparts. As shown in Fig. 6, the d–d band of $NiSO_4$ in methanol does not shift upon addition of BIH or BSIH, but does shift considerably upon addition of BASIH. The shift in absorbance coincides with considerable precipitate formation, which is not observed with BIH or BSIH and Ni^{2+}. As with the other metal ions, an intense color change accompanies the addition of SIH to Ni^{2+}, with considerable precipitation of an orange solid. In the case of Zn^{2+}, mixtures with BSIH or BIH

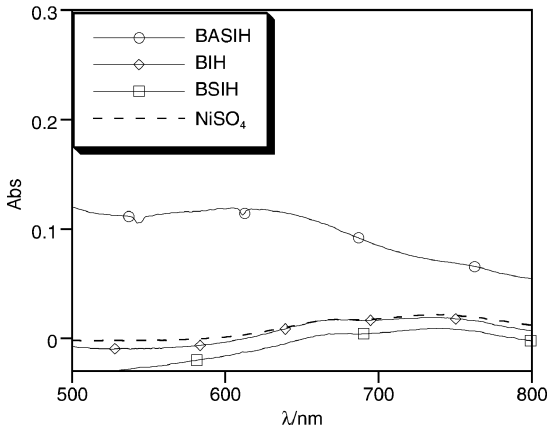

Fig. 6 Visible spectra of 10 mM methanol solutions of $NiSO_4$ with 10 mM added BASIH, BIH, or BSIH. The d–d band of Ni^{2+} is most affected by the addition of BASIH.

remain clear, while those with BASIH become cloudy and with SIH considerable precipitate forms.

These studies suggest that boronic ester analogs of this class of pro-chelators will be preferable for future *in vivo* studies in order to prevent unwanted interactions with metal ions prior to activation to the chelator form.

Relative stability of iron complexes

The thermodynamic stability of iron–chelator complexes is one of several important properties that can influence the therapeutic application of these molecules.[14] Although pre-organized, hexadentate ligands generally have very high affinities for Fe^{3+}, their large size can limit their access across cellular membranes. The smaller, tridentate chelators of the PIH/SIH family have molecular weights under 500, but retain strong affinity for ferric iron. The pre-organization of the 3 donor atoms described in the structural analysis above is likely a contributing factor to the stability of these complexes. A direct comparison of overall formation constants is complicated when comparing ligands of varying pK_a's and different binding stoichiometries, therefore it is often useful to compare pFe ($-\log[Fe_{aq}^{3+}]$) values, which provide an assessment of the amount of uncomplexed iron that would be available at pH 7.4 with total ligand and iron concentrations of 10 μM and 1 μM, respectively.[36] Variations of reported pFe values for SIH and PIH ligands range from 23 to 50.[37–39] For comparison, the pFe of EDTA is 25.1, while that of desferrioxamine is 26.6.[36] Although the very high value for SIH is unrealistic since it is known not to compete with desferrioxamine, the range gives an indication of the effectiveness of this class of chelators. The wide discrepancy in their pFe values arises from difficulties encountered with measuring accurate stability constants for these compounds due to solubility problems as well as hydrolysis of the ligands under the extreme low and high pH values accessed during typical potentiometric titrations.[38–40]

In this study, we chose to estimate the relative binding ability among our series of chelators by monitoring the competition between FeL_2 and EDTA in solution conditions of 20 mM phosphate buffer at pH 7.4 with 50% methanol and 500 mM NaCl. Methanol was added as a co-solvent to ensure that all species stayed in solution. Initial solutions of Fe^{3+} and 3-fold excess ligand were prepared to ensure complete formation of FeL_2, which was monitored by its absorbance at 480 nm. In the case of SIH, we found that a 1 : 3 : 10 ratio of Fe^{3+} : SIH : EDTA resulted in a decrease of the initial $[Fe(SIH)_2]^+$ concentration to just under 50%, as shown by the bar graph in Fig. 7. These same concentrations and ratios were then used for the other analogs in order to establish their relative affinity compared to SIH.

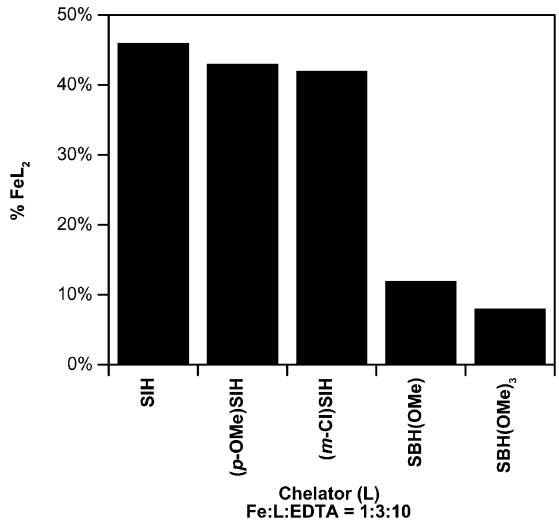

Fig. 7 Percentage of the $[FeL_2]^+$ species (as monitored at 480 nm), that persists in solutions containing 0.15 mM $FeCl_3$, 0.45 mM chelator (L), and 1.5 mM EDTA (Fe : L : EDTA = 1 : 3 : 10) equilibrated overnight in 50 : 50 methanol–phosphate buffer (20 mM, with 500 mM NaCl, pH 7.4).

The data in Fig. 7 show that altering the electronic nature of the phenol-containing ring with either an electron-donating methoxy group or an electron-withdrawing chloro group has little influence on the relative stability of the chelators. Both (*p*-OMe)SIH and (*m*-Cl)SIH retain 40–45% of their iron when challenged with EDTA under these conditions. In contrast, both of the SBH derivatives investigated retain only about 10% of their signal, indicating that they are weaker binders compared with the SIH analogs.

These data collectively indicate that the electron-donating pyridine ring of SIH derivatives plays a significant role in stabilizing high affinity Fe^{3+} complexes. The data also corroborate prior studies by placing SIH higher than EDTA on a relative pFe scale.

Kinetics of pro-chelator to chelator conversion

Since the rates of conversion of the pro-chelators to their active chelator versions will have important ramifications for their potential biological applications, we compared the oxidation rates of analogs BSIH, BASIH, $BSBH(MeO)_3$, (*p*-OMe)BASIH, and (*m*-Cl)BASIH under pseudo first-order conditions of excess H_2O_2. In order to keep all of the pro-chelators and chelators in solution during these reactions, all kinetic runs were carried out in a mixed solvent system of 50% methanol, 50% 20 mM phosphate buffer at pH 7.4. Reactions were monitored spectrophotometrically. Fig. 8 shows the conversion of 50 μM (*p*-OMe)BASIH to (*p*-OMe)SIH with 1 mM H_2O_2 as a representative example of a typical kinetics run. The isosbestic points at 270 and 330 nm indicate clean conversion between the two species. As shown in Fig. 9, the observed pseudo first-order rate constants (k_{obs}) show a linear

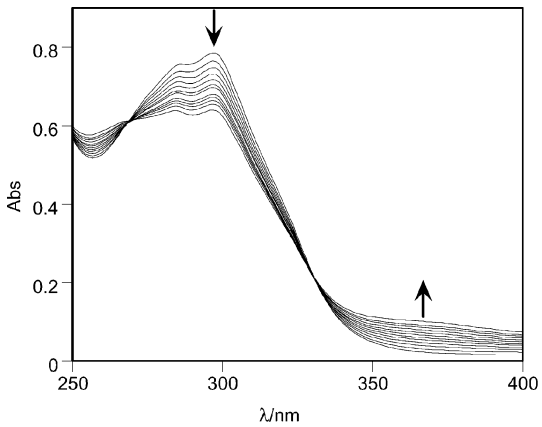

Fig. 8 Conversion of 50 μM (*p*-OMe)BASIH to (*p*-OMe)SIH by oxidation with 1 mM H_2O_2 in 50 : 50 MeOH–20 mM phosphate buffer, pH 7.4. The spectra represent the first 30 min of the reaction.

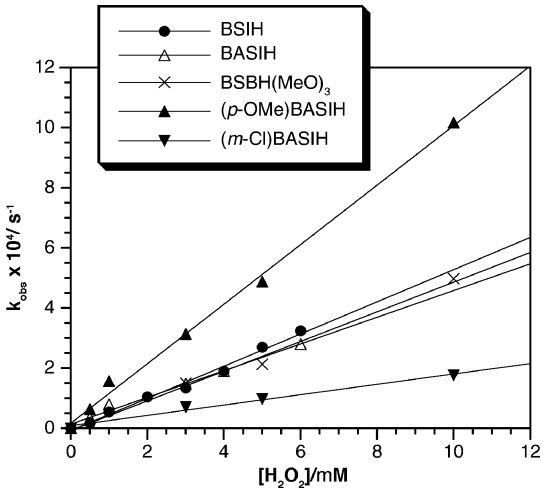

Fig. 9 Plots of k_{obs} *vs* H_2O_2 concentration for the conversion of the listed pro-chelators to their respective chelator version. The second-order rate constant, k, was obtained from the slope of these lines: BSIH $k = 0.053$, BASIH $k = 0.044$, $BSBH(MeO)_3$ $k = 0.049$, (*p*-OMe)BASIH $k = 0.077$, (*m*-Cl)BASIH $k = 0.017$ M^{-1} s^{-1}.

dependence on the concentration of H_2O_2; the second-order rate constant (k) for each analog was obtained from the slope of this line.

A comparison of the data shown in Fig. 9 reveals that changing the boronic ester functionality of BSIH ($k = 0.053$ M^{-1} s^{-1}) to the boronic acid analog BASIH ($k = 0.044$ M^{-1} s^{-1}) has little influence on the rate of H_2O_2-dependent oxidation to the phenol. Likewise, modifying the aroyl ring, as in the case of $BSBH(MeO)_3$ ($k = 0.049$ M^{-1} s^{-1}), has little influence on the conversion rate. Chemically modifying the boron-containing aryl ring, however, causes significant changes to the rate. For example, placing an electron-donating methoxy group *para* to the boronic acid in (*p*-OMe)BASIH results in a 1.45-fold acceleration ($k = 0.077$ M^{-1} s^{-1}). In contrast, the electron-withdrawing chloro substituent in (*m*-Cl)BASIH slows the reaction down 3-fold ($k = 0.017$ M^{-1} s^{-1}).

In order to test the stability of the pro-chelators in conditions that may be used for future cell culture experiments, the pro-chelators were dissolved in 100 mM aqueous NaOH and frozen for 48 h. No changes in the UV-vis spectrum were noted after the solutions were defrosted and allowed to sit at room temperature for at least 4 h, indicating their stability under these conditions.

Inhibition of hydroxyl radical formation

We have previously shown that the H_2O_2-activated pro-chelator BSIH inhibits the production of $OH^{\bullet}$ produced under Fenton conditions nearly as effectively as the chelator SIH itself.[18] In order to test how the chemical modifications on the BSIH framework influence this property, we subjected the new pro-chelators (*m*-Cl)BASIH, (*p*-OMe)BASIH, and BSBH(*m*-OMe) to the deoxyribose assay in order to compare them with BSIH and SIH. In this assay, hydroxyl radicals generated by reaction of reduced iron and H_2O_2 degrade 2-deoxyribose into by-products that are monitored spectrophotometrically after reaction with thiobarbituric acid (TBA).[41] Chelating agents that prevent the metal from reacting with H_2O_2 result in a decrease in absorption of the TBA-reactive species at 532 nm. Quenchers that scavenge hydroxyl radicals also decrease the amount of TBA-reactive species, although usually at higher concentrations compared to effective chelating agents.

The data shown in Fig. 10 are presented as the ratio of the absorbance at 532 measured in the presence (A) or absence (A_o) of chelator or pro-chelator. A/A_o values below 1 indicate protection against deoxyribose degradation, whereas values above 1 suggest an enhancement of metal-mediated radical formation. Both BSIH and SIH provide nearly maximal protection against deoxyribose degradation under these conditions with pro-chelator concentrations as low as 50 μM. The BSBH analog, however, does not achieve this level of protection until 200 μM of the pro-chelator has been added. In addition, the slight increase in A/A_o above 1 suggests that low concentrations of an SBH chelator may actually support iron in an environment that promotes Fenton chemistry, for example *via* mono-chelated binding. The behavior of the BSBH(*m*-OMe) observed in the deoxyribose assay is consistent

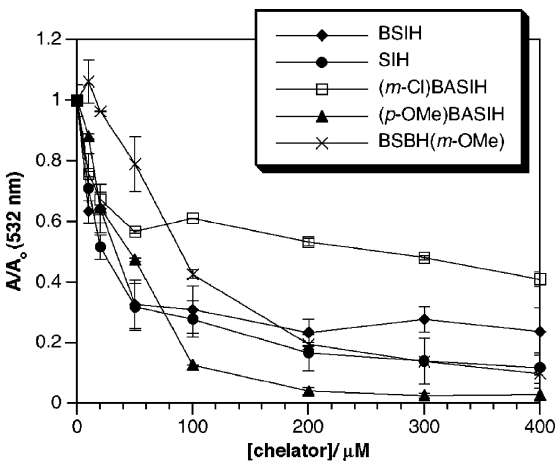

Fig. 10 Dependence of pro-chelator concentration on deoxyribose degradation by hydroxyl radicals generated under Fenton conditions (200 μM H_2O_2, 10 μM $FeCl_3$, 2 mM ascorbic acid, 15 mM 2-deoxyribose in pH 7.4 phosphate buffer). A and A_o are the absorbance readings at 532 nm with and without added chelator. Values of $A/A_o < 1$ signify protection against deoxyribose degradation by $OH^{\bullet}$.

with the results described in the previous section that indicate SBH analogs are weaker iron binders compared to the SIH analogs.

A comparison of (*m*-Cl)BASIH and (*p*-OMe)BASIH shows that the rate of H_2O_2 activation does indeed correlate with the overall inhibition of $OH^{\bullet}$ formation. The *p*-OMe derivative provides the fastest conversion from pro-chelator to chelator, and as shown in Fig. 10 also provides the most protection against deoxyribose degradation. In contrast, the *m*-Cl derivative is unmasked by H_2O_2 nearly 5 times slower than the *p*-OMe version, and after an hour of being subjected to Fenton conditions in the deoxyribose assay, this analog provides only modest protection. BSIH, which has a rate constant in between these two derivatives, also shows an intermediate level of protection. Given the rate constants obtained from Fig. 9, only 2.4 μM of the (*m*-Cl)SIH would be present from 200 μM pro-chelator at the time the reactions are monitored. In contrast, nearly 8 μM SIH and 11 μM (*p*-OMe)SIH would be available. It is important to note that the reaction conditions used for the kinetic analysis in Fig. 9 and the deoxyribose assay in Fig. 10 are different, so these calculations only provide relative estimates of predicted concentrations. Overall, the trend in the protective effect of the pro-chelators mirrors their reactivity with H_2O_2, with the more readily unmasked analogs providing the maximum inhibition of $OH^{\bullet}$ formation.

Copper is another biologically important metal ion that can undergo Fenton-like reactions depending on its coordination environment, and although its concentration in cells is lower than that of iron, it is a more effective catalyst for $OH^{\bullet}$ generation.[1] SIH is known to inhibit copper-mediated $OH^{\bullet}$ formation,[42] a conclusion verified in our studies for comparison purposes, as shown by the deoxyribose degradation data presented in Fig. 11. BSIH also shows a protective effect, although complete suppression of TBA-reactive species is never fully achieved, even in the presence of 40-fold excess chelator to copper, the highest ratio tested. As shown in Fig. 11, desferrioxamine (DFO) provides 80–90% protection when present in concentrations equivalent or higher than copper (10 μM). This effect is slightly better than SIH, which provides about 75% protection above 20 μM, and BSIH, which shows about 65% protection above 50 μM. The boronate-masked salicylaldehyde Bsal ((2-formylphenyl)boronic acid pinacol ester) does not show an effect on the A/A_o value until the highest concentrations, indicating that consumption of H_2O_2 *via* reaction with the aryl boronic ester functionality is not the source of the protective effect of the pro-chelator in this assay.

In the absence of added H_2O_2, mixtures of copper and ascorbic acid in air are still capable of generating $OH^{\bullet}$. Whereas SIH and DFO are effective chelators for inhibiting these reactions (data not shown), BSIH is only effective at concentrations greater than 200 μM, as shown in Fig. 11. Since H_2O_2 is required to convert BSIH to its tridentate chelator SIH,[18] it is likely that this moderate protective effect is due to complex formation between BSIH itself and copper. As described above, BSIH–Cu complexes are weak, therefore relatively high concentrations of the ligand are required to form a complex that disfavors Fenton-type reactions.

To test this hypothesis further, BIH was also tested in the deoxyribose assay (in the presence of H_2O_2). As shown in Fig. 11, its behavior tracks very similarly to that of BSIH without H_2O_2. These data support the conclusion that the potentially bidentate hydrazone functionality of this class of compounds interacts with copper.

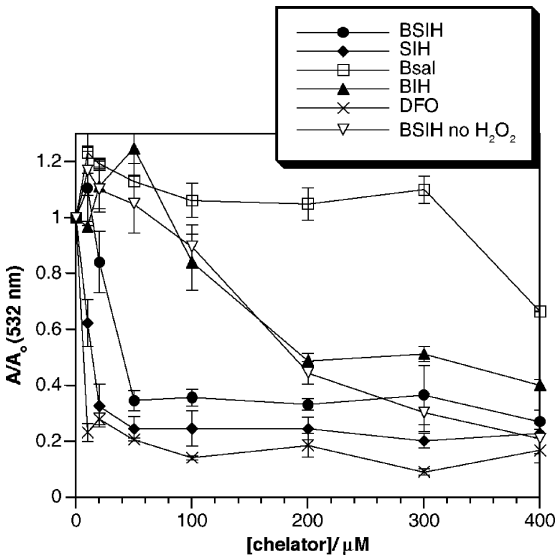

Fig. 11 Dependence of pro-chelator concentration on deoxyribose degradation by hydroxyl radicals generated under copper-induced Fenton conditions (100 μM H_2O_2, 10 μM $CuSO_4$, 2 mM ascorbic acid, 15 mM 2-deoxyribose in pH 7.4 phosphate buffer). BSIH was also tested without addition of H_2O_2 ("BSIH no H_2O_2"). A and A_o are the absorbance readings at 532 nm with and without added chelator. Values of $A/A_o < 1$ signify protection against deoxyribose degradation by $OH^{\bullet}$. Bsal is (2-formylphenyl)boronic acid pinacol ester, which was used as a control to demonstrate that the reaction of a boronic ester with H_2O_2 alone does not provide the protective effect observed for the chelators.

Partition coefficients

A compound's ability to permeate biological membranes *via* passive diffusion is partly a function of its lipophilicity, which is conveniently assessed by its partition coefficient, *P*, between *n*-octanol and water.[43] While several computer programs are available to calculate partition coefficients based on molecular fragments, such calculations for aroyl hydrazones can differ from experimental values by as much as 3 log units.[44] We therefore chose to measure these values directly in an octanol–buffer system.

Table 4 lists the log *P* values assembled for several of the compounds in Fig. 1 and their corresponding bis-ligated ferric complexes. All of the compounds studied are moderately hydrophobic, with log *P* values ranging from 1.9 to 2.9. The pro-chelators (BL) as a trend are less lipophilic than either their free ligand (L) or their iron complex (FeL_2). This trend is reversed for the trimethoxy SBH derivative, where $BSBH(OMe)_3$ has a log *P* of 2.9, while its chelator and iron complex have log *P* values of 2.5.

The biological activity of iron chelators to mobilize iron from cellular stores has been found to correlate to the lipophilicity

Table 4 Octanol/water partition coefficients (log *P*) of chelators (L), pro-chelators (BL) and iron complexes $[FeL_2]^+$

log *P* (octanol–water)	L	(BL)	$[FeL_2]^+$
SIH	2.4	2.3[a] 1.9[b]	2.4
SBH(*m*-OMe)	2.9	2.3	2.4
SBH(*m*-OEt)	2.9	2.3	2.9
$SBH(OMe)_3$	2.5	2.9	2.5

[a] BSIH. [b] BASIH.

of both the free ligands and their iron complexes.[44–48] For aroyl hydrazones, ligands with log P_L ~2.8 and a log P_{FeL} ~3.1 show optimal iron mobilization activity.[44] The parent BSIH pro-chelator with log $P = 2.3$ falls slightly below this optimal range, but the data in Table 4 show that modifications to the parent compound can be made to increase the lipophilicity of the pro-chelators.

Conclusions

In an effort to improve the utility of medicinal metal chelators, we have introduced a pro-chelator strategy in which metal-binding ligands are masked by protecting groups that are released under conditions of oxidative stress to expose high-affinity ligands. Here, we have introduced a series of pro-chelators in which modifications to the aroyl hydrazone framework of the parent BSIH compound tune their properties and reactivity. For example, replacing the boronic ester masking group by a boronic acid reduces the lipophilicity of the pro-chelator, but does not affect the rate of H_2O_2-dependent conversion to the chelator. Neither the boronic ester nor the boronic acid versions interact significantly with Fe^{3+}, although the boronic acid versions do form methanol-insoluble precipitates with divalent metal ions such as Cu^{2+}, Zn^{2+}, and Ni^{2+}. The boronic ester versions are therefore likely to be more favorable for future medicinal or biological applications, as it will be desirable to avoid premature metal binding. In addition, boronic acids readily bind vicinal diols such as carbohydrates,[49] which could further complicate the availability of the chelator.

Replacing the pyridine ring of the SIH framework with an aryl ring of SBH decreases the Fe^{3+} binding affinity of the ligand, which in turn lowers its efficacy to inhibit iron-promoted hydroxyl radical formation. The electron-donating nature of the N atom in the pyridine ring provides more electron density on the carbonyl O donor for improved metal binding. In terms of metal affinity, this modification has more influence than changing the electronic nature of the opposing phenol ring. As assessed by EDTA competition studies, very little difference in relative iron affinity was observed between the electron-donating *p*-OMe and the electron-withdrawing *m*-Cl derivatives. Future studies will be required to provide a more quantitative evaluation of binding affinity.

Where these modifications do have significant impact is in the rate of H_2O_2-dependent conversion from the pro-chelator to the chelator. A substituent that is electron-donating with respect to the boron accelerates this rate, while an electron-withdrawing group slows it down. In moving from (*p*-OMe)BASIH to BASIH to (*m*-Cl)BASIH, a nearly 5-fold difference in conversion rate is observed. This range is highly advantageous for future biological and medicinal studies, since the advantage of the pro-chelators will be linked to their triggered activation only under conditions of oxidative stress. Increasing the rate is clearly linked to improved protection against metal-promoted oxidative stress. On the other hand, analogs with slower rates will be more robust in avoiding untimely chelator release by harmless background levels of H_2O_2.

How these chemical modifications affect *in vivo* function will be a key step in validating the pro-chelator strategy for inhibiting metal-promoted oxidative stress and is the subject of future investigations.

Experimental

General considerations

Chemicals were obtained from Fisher Scientific or Acros Organics and used without further purification unless otherwise noted; (2-formylphenyl)boronic acid pinacol ester was purchased from Combi-Blocks, Inc; (5-chloro-2-formylphenyl)boronic acid and (4-methoxy-2-formylphenyl)boronic acid were purchased from Matrix Scientific. SIH,[50,51] BSIH, and $[Fe(SIH)_2]NO_3$ were prepared as described previously.[18] All solvents were reagent grade and all aqueous solutions were prepared from nanopure water. UV-vis spectra were recorded on a Phototonics Model 420 Fiber Optic CCD Array UV-vis spectrophotometer. ^{1}H and ^{13}C NMR spectra were recorded on a Varian Mercury 300, Inova 400 or 500 spectrometer; δ values are in ppm and J values are in Hz. IR Spectra were recorded on a Nicolet 360 FT-IR. Ionization mass spectrometry (ESI-MS) was preformed on an Agilent 1100 Series LC/MSD trap spectrometer with a Daly conversion dynode detector. Samples were infused *via* a Harvard apparatus syringe pump at 33 μL min^{-1}. Ionization was achieved in the positive- or negative-ion mode by application of +5 or −5 kV at the entrance to the capillary; the pressure of the nebulizer gas was 20 psi. The drying gas was heated to 325 °C at a flow rate of 7 L min^{-1}. Full-scan mass spectra were recorded in the mass/charge (m/z) range of 100–2000. Elemental analysis was performed by Desert Analytics/TransWest Geochem, Tucson, AZ.

Synthesis

BASIH. Isonicotinic acid hydrazide (1 mmol, 0.137 g) was dissolved in 2 mL of 0.1 M sodium acetate buffer (pH 4.5) and added to a solution of (2-formylphenyl)boronic acid (1 mmol, 0.145 g) dissolved in 1 mL of methanol. The reaction was stirred for 5 min at 100 °C and cooled over ice. The white precipitate was collected *via* vacuum filtration, washed with water and dried *in vacuo* to yield a white powder (215 mg, 80%). ^{1}HNMR (CD_3OD 400 MHz): δ 7.34 (3H, m), 7.56 (1H, s), 7.84 (2H, d, $J = 5.88$), 8.42 (1H, s), 8.71(2H, d, $J = 5.98$). ^{13}CNMR (CD_3OD 101 MHz): δ 121.94, 128.57, 129.98, 131.23, 149.82, 150.75. ESI-MS: m/z 267.8 (M − H)$^-$, 292 (M + Na)$^+$. IR (neat, ν_{max}/cm^{-1}): 3204, 3056, 2360, 1547, 1379, 1357, 1338, 1195, 1168, 1145, 766, 693. λ_{max}(MeOH)/nm 302 (ε/dm^3 mol^{-1} cm^{-1} 15 800); λ_{max}(octanol) 258 (7800), 300 (9300).

(*p*-OMe)BASIH. A similar procedure to the one described above for BASIH was followed, but replacing (2-formylphenyl)-boronic acid with 4-methoxy-2-formylphenylboronic acid. A white powder was isolated in 70% yield. ^{1}HNMR (CD_3OD 400 MHz): δ 3.83 (3H, s), 6.98 (1H, dd, $J = 8.14, 2.30$), 7.28 (1H, d, $J = 8.15$), 7.36 (1H, d, $J = 2.15$), 7.84 (2H, d, $J = 5.75$), 8.41 (1H, s), 8.71 (2H, d, $J = 5.08$). ^{13}CNMR (CD_3OD 101 MHz): δ 54.55, 112.77, 116.07, 121.95, 132.79, 149.84, 150.70. ESI-MS: m/z 322.0 (M + Na)$^+$, 297.8 (M − H)$^-$. IR (neat, ν_{max}/cm^{-1}): 2204, 1647, 1552, 1358, 748, 618. λ_{max}(MeOH)/nm 320 (ε/dm^3 mol^{-1} cm^{-1} 19 700).

(*p*-OMe)SIH. A portion of (*p*-OMe)BASIH (0.5 mmol, 150 mg) was dissolved in 10 mL of MeOH. As H_2O_2 (11 mmol, 0.62 mL 50% H_2O_2) was added dropwise to the solution, the reaction mixture turned clear yellow. After stirring for 2 h, solvent was removed *in vacuo* to yield a yellow powder (123 mg, 91%). ^{1}HNMR

(CD_3OD 400 MHz): δ 3.74 (3H, s), 6.81 (1H, d, $J = 8.94$), 6.89 (1H, dd, $J = 8.96, 3.02$), 7.06 (1H, d, $J = 2.99$), 7.85 (2H, dd, 4.58, 1.57), 8.51 (1H, s), 8.71 (2H, d, $J = 5.84$). ^{13}CNMR (CD_3OD 101 MHz): δ 55.14, 117.38, 118.31, 119.23, 122.15, 149.86, 152.95. ESI-MS: m/z 269.9 $(M - H)^-$.

(*m*-Cl)BASIH. A similar procedure to the one described above for BASIH was followed, but replacing (2-formylphenyl)boronic acid with 5-chloro-2-formylphenylboronic acid. A white powder was isolated in 78% yield (236 mg). ^{1}HNMR (CD_3OD 400 MHz): δ 7.33 (1H, s), 7.40 (1H, d, $J = 7.82$), 7.60 (1H, d, $J = 6.75$), 7.84 (2H, d, $J = 2.28$), 8.40 (1H, s), 8.71 (2H, s). ESI-MS: m/z 325.9 $(M + Na)^+$ 301.8 $(M - H)^-$. IR (neat, ν_{max}/cm^{-1}): 3294, 2158, 2023, 1653, 1581, 1340, 1306, 1024, 704, 689. λ_{max}(MeOH)/nm 302 (ε/dm^3 mol^{-1} cm^{-1} 21 500).

(*m*-Cl)SIH. A similar procedure to the one described above for (*p*-OMe)SIH was followed, but replacing (*p*-OMe)BASIH with (*m*-Cl)BASIH. A yellow powder was isolated in 89% yield (122 mg). ^{1}HNMR (CD_3OD 400 MHz): δ 6.91 (2H, m), 7.46 (1H, d, $J =$ 8.05), 7.85 (2H, d, $J = 4.47$), 8.51 (1H, s), 8.72 (1H, s). ESI-MS: m/z 273.9 $(M - H)^-$.

BIH. Equimolar quantities of isonicotinic acid hydrazide (1 mmol, 0.137 g) and benzaldehyde (1 mmol, 0.102 mL) were dissolved in 2 mL of 0.1 M sodium acetate buffer (pH 4.5); the reaction was stirred for 5 min at 100 °C and cooled over ice. The white precipitate was collected *via* vacuum filtration, washed with water and dried *in vacuo* to yield 153 mg of a white precipitate (67% yield). ^{1}HNMR (CD_3OD 400 MHz): δ 7.41 (3H, m), 7.81 (1H, dd, $J = 6.68, 2.97$), 7.86 (2H, dd, $J = 4.51, 1.67$), 8.33 (1H, s), 8.71 (2H, dd, $J = 4.54, 1.64$). ^{13}CNMR (CD_3OD 101 MHz): δ 121.95, 127.75, 128.65, 130.72, 134.01, 141.22, 149.89, 150.67. ESI-MS m/z 223.8 $(M - H)^-$, 247.9 $(M + Na)^+$. IR (neat, ν_{max}/cm^{-1}): 2357, 2172, 2000, 1684, 1564, 1285, 686. λ_{max}(MeOH)/nm 301 (ε/dm^3 mol^{-1} cm^{-1} 19 500).

BSBH(*m*-OMe). One equivalent of (2-formylphenyl)boronic acid pinacol ester was added *via* syringe to a 2-mL solution of 3-methoxybenzhydrazide (1 mmol, 166 mg) in methanol and heated to 60 °C. After stirring for 10 min, 1 mL of chilled diethyl ether was added and the reaction was placed over ice. A white precipitate was collected *via* vacuum filtration, washed with diethyl ether, and dried *in vacuo* to provide 284 mg of a white powder (72% yield). ^{1}HNMR (DMSO, 500 MHz δ ppm 1.33 (12H, s), 3.83 (3H, s), 7.16 (1H, d, $J = 7.39$ Hz), 7.45 (4H, m), 7.54 (1H, t, $J = 7.40$ Hz), 7.71 (1H, d, $J = 7.31$ Hz), 8.01 (1H, d, $J = 7.81$ Hz), 8.94 (1H, s), 11.96 (1H, s) ^{13}CNMR (DMSO 125 MHz): δ 24.51, 55.25, 83.83, 113.06, 117.17, 119.87, 125.47, 128.85, 129.54, 130.93, 135.00, 135.38, 139.54, 148.31, 159.06, 163.25. ESI-MS m/z 381.1 $(M + H)^+$. IR (neat, ν_{max}/cm^{-1}): 3204, 3060, 2963, 1643, 1589, 1544, 1482, 1349, 1276, 1136, 1056, 965, 862, 805, 758, 695, 655. λ_{max}(MeOH)/nm 298 (ε/dm^3 mol^{-1} cm^{-1} 22 600).

SBH(*m*-OMe). One equivalent of salicylaldehyde was added to a 2-mL solution of 3-methoxybenzhydrazide (0.5 mmol, 83 mg) in methanol in a 10-mL round bottomed flask. The reaction was stirred for 10 min at 60 °C and cooled over ice. White needle-like crystals suitable for X-ray diffraction were collected *via* vacuum filtration (98 mg, 74% yield). ^{1}H NMR (DMSO, 400 MHz δ ppm 3.83 (3 H, s), 6.93 (2 H, m), 7.17 (1 H, d, $J = 7.86$), 7.30 (1 H, t, $J = 7.67$), 7.45 (2 H, m), 7.53 (2 H, m), 8.65 (1 H, s), 11.29 (1 H, s), 12.08 (1 H, s). ^{13}CNMR (DMSO, 101 MHz δ ppm 55.28, 112.79, 116.34, 117.64, 118.6, 119.27, 119.75, 129.41, 129.66, 131.32, 134.09, 148.25, 157.38, 159.17, 162.47. ESI-MS m/z 268.9 $(M - H)^-$, 293.1 $(M + Na)^+$. IR (neat, ν_{max}/cm^{-1}): 3450, 2244, 1668, 1283, 816, 754. λ_{max}(octanol)/nm 288 (ε/dm^3 mol^{-1} cm^{-1} 18 700), 332 (13 700).

BSBH(*m*-OEt). One equivalent of (2-formylphenyl)boronic acid pinacol ester was added to a 2-mL solution of 3-ethoxybenzhydrazide (1 mmol, 185 mg) in ethanol and heated to 60 °C. After stirring for 10 min, the solvent was removed *in vacuo*. The white solid was washed with diethyl ether and dried *in vacuo* to give 200 mg of a white powder (50% yield). ^{1}HNMR: (DMSO, 500 MHz): δ 1.35 (15H, s), 3.32 (1H, s), 4.09 (2H, q, $J = 6.8$), 7.14 (1H, d, $J = 7.45$), 7.43 (4H, m), 7.54 (1H, t, 7.38), 7.71 (1H, d, $J =$ 7.31), 8.00 (1H, d, $J = 7.74$), 8.93 (1H, s), 11.93 (1H, s). ^{13}C NMR (DMSO 125 MHz): δ 14.51, 24.51, 63.2, 83.83, 113.59, 117.47, 119.79, 125.49, 128.84, 129.55, 130.94, 134.96, 135.39, 139.57, 148.26, 158.32, 163.25. ESI-MS m/z 395.1 $(M + H^+)$. IR (neat, ν_{max}/cm^{-1}): 3199, 2978, 1642, 1548, 1479, 1346, 1273, 1139, 1050, 965, 857, 806, 762, 655. λ_{max}(MeOH)/nm 298 (ε/dm^3 mol^{-1} cm^{-1} 20 000).

SBH(*m*-OEt). A similar procedure to the one described above for SBH(*m*-OMe) was followed on a 0.5 mmol scale, but using 3-ethoxybenzhydrazide. 93 mg of a white powder product was isolated (65% yield). ^{1}HNMR (DMSO, 400 MHz): δ 1.35 (3H, t, $J = 6.8$), 4.10 (2H, q, $J = 6.8$), 6.92 (2H, m), 7.14 (1H, d, $J =$ 7.6), 7.16 (1H, t, $J = 7.6$), 7.46 (4H, m), 8.64 (1H, s), 11.28 (1H, s), 12.05 (1H, s). ^{13}CNMR (DMSO 101 MHz): δ 14.51, 63.24, 113.3, 116.33, 117.93, 118.58, 119.25, 119.66, 129.42, 129.66, 131.3, 134.02, 148.22, 157.38, 158.42, 162.43. ESI-MS m/z 285.1 $(M + H^+)$, 307.2 $(M + Na^+)$. IR (neat, ν_{max}/cm^{-1}): 3191, 3056, 1649, 1599, 1548, 1481, 1357, 1293, 1238, 1137, 1082, 957, 816, 723, 680. λ_{max}(MeOH)/nm 288 (ε/dm^3 mol^{-1} cm^{-1} 22,200), 298 (21 200), 330 (16 000).

BSBH(OMe)$_3$. A similar procedure to the one described above for BSBH(*m*-OMe) was followed, but using 3,4,5-trimethoxybenzhydrazide. A white powder (550 mg) was isolated in 81% yield. ^{1}HNMR (DMSO, 500 MHz): δ ppm 1.33 (12H, s), 3.72 (3H, s), 3.86 (6H, s), 7.19 (2H, s), 7.43 (1H, t, $J = 5.51$), 7.54 (1H, m), 7.71 (1H, d, $J = 6.53$), 7.98 (1H, d, $J = 5.89$), 8.92 (1H, s), 11.84 (1H, s). ^{13}CNMR (DMSO 75 MHz): δ 24.52, 56.03, 60.04, 83.84, 105.34, 125.62, 128.81, 130.92, 135.34, 139.47, 140.27, 148.35, 152.56, 163.02. ESI-MS m/z 441.1 $(M + H)^+$. IR (neat, ν_{max}/cm^{-1}): 2965, 1651, 1584, 1501, 1453, 1414, 1324, 1269, 1228, 1142, 1123, 1062, 1003, 858, 777, 726. λ_{max}(MeOH)/nm 300 (ε/dm^3 mol^{-1} cm^{-1} 25 100).

SBH(OMe)$_3$. A similar procedure to the one described above for SBH(*m*-OMe) was followed, but using 3,4,5-trimethoxybenzhydrazide. 185 mg of a white powder was isolated (56% yield). ^{1}HNMR (DMSO, 400 MHz): δ ppm 3.73 (3H, s), 3.86 (6H, s), 6.92 (2H, t, $J = 8.63$), 7.29 (3H, m), 7.55 (1H, d, $J = 7.38$), 8.65 (1H, s), 11.24 (1H, s), 11.94 (1H, s). ^{13}CNMR (DMSO, 101 MHz): δ ppm 38.80, 39.01, 39.22, 39.43, 39.64, 39.85, 40.06, 56.02, 60.05, 105.14, 116.31, 118.67, 119.27, 127.79, 129.21, 131.29, 140.50, 147.83, 152.65, 157.31, 162.13. ESI-MS m/z 331.2 $(M + H^+)$, 353.2 $(M + Na^+)$. IR (neat, cm^{-1}): 2996, 1643, 1573, 1495, 1452, 1410, 1330,

1227, 1119, 996, 851, 678. λ_{max}(MeOH)/nm 290 (ε/dm^3 mol^{-1} cm^{-1} 24 500), 300 (25 500), 330 (19 300).

Fe complexes

The iron complexes of the SBH derivatives were prepared by refluxing 2 equivalents of the ligand with one equivalent of $Fe(NO_3)_3 \cdot 9H_2O$ in methanol for one hour, as described previously for $[Fe(SIH)_2](NO_3)$.[18]

[Fe(SBH(*m*-OMe))$_2$](NO$_3$). ESI-MS *m*/*z* 594.0 (M^+). IR (neat, ν_{max}/cm^{-1}): 2978, 1602, 1549, 1433, 1387, 1321, 1303, 1244, 1205, 1149, 1089, 1032, 905, 821, 803, 731. λ_{max}(MeOH)/nm 297 (ε/dm^3 mol^{-1} cm^{-1} 24 000), 338 (12 500). Elemental Analysis calc. for $C_{30}H_{26}FeN_5O_9$: C, 54.9; H, 4.0; N, 10.7; found: C, 54.7; H, 4.1; N, 10.6%.

[Fe(SBH(*m*-OEt))$_2$](NO$_3$). ESI-MS *m*/*z* 622.0 (M^+). IR (neat, ν_{max}/cm^{-1}): 2936, 1606, 1536, 1385, 1341, 1312, 1245, 1125, 990, 910, 834, 758. λ_{max}(MeOH)/nm 296 (ε/dm^3 mol^{-1} cm^{-1} 31 300), 338 (15 700). Elemental Analysis calc. for $C_{32}H_{30}FeN_5O_9 \cdot H_2O$: C, 54.7; H, 4.6; N, 10.0; found: C, 55.2; H, 4.6; N, 9.8%.

[Fe(SBH(OMe)$_3$)$_2$](NO$_3$). Black needle crystals suitable for X-ray diffraction were grown in a 6 mm glass tube by slow diffusion of pentane into a saturated solution of $[Fe(SBH(OMe)_3)_2](NO_3)$ dissolved in chlorobenzene. ESI-MS *m*/*z* 714.1 (M^+). IR (neat, ν_{max}/cm^{-1}): 2927, 1605, 1543, 1501, 1386, 1339, 1311, 1242, 1124, 992, 832, 755. λ_{max}(MeOH)/nm 300 (ε/dm^3 mol^{-1} cm^{-1} 41 100), 338 (24 700). Elemental Analysis calc. for $C_{34}H_{34}FeN_5O_{13} \cdot H_2O$: C, 51.4; H, 4.3; N, 8.8; found: C, 51.2; H, 4.65; N, 8.75%.

Ligand–metal selectivity

The interaction of ligands BSIH, BASIH, BIH and SIH with $NiSO_4$, $Fe(NO_3)_3$, $CuSO_4$ and $Zn(OAc)_2$ were studied. In a typical reaction, the metal (10 mM) was added to a solution of ligand (10 mM) in methanol. The solutions were allowed to equilibrate and any precipitation due to metal–ligand complexation was noted. UV-vis spectra were collected for the reaction mixtures that did not precipitate or for the supernatants of mixtures in which precipitate formed.

Determination of relative conditional stability by EDTA competition

Solutions containing a 1 : 3 ratio of $FeCl_3$ (0.15 mM) to ligand L (0.45 mM) were prepared in 10 mL of 50 : 50 (v/v) methanol : $NaHPO_4$ buffer (pH = 7.4) containing 500 mM NaCl. The Fe^{3+} was added from a methanol stock solution to the prepared ligand solution to avoid precipitation of iron hydroxides at pH 7.4. An initial absorbance reading at 480 nm was measured to indicate the total amount of $[FeL_2]^+$ present. A 10-fold excess (with respect to Fe) of EDTA (1.5 mM) was added, and the solutions were allowed to equilibrate for > 12 h in the dark. A final absorbance reading at 480 nm was measured to indicate the remaining $[FeL_2]^+$ species was still present in the presence of competing EDTA (Fe–EDTA species have no absorbance at 480 nm).

Kinetics

The rates of oxidation of the pro-chelators to their respective chelator were investigated under pseudo first-order conditions of excess H_2O_2. In a typical kinetic study, 3 mL of a 30 μM solution of the pro-chelator in 50 : 50 (v/v) methanol–$NaHPO_4$ buffer (20 mM, pH = 7.4) were loaded into a quartz cuvette. Upon addition of H_2O_2 (300 μM–10 mM) to the mixture, spectra were taken at time increments such that a minimum of 30 spectra were collected throughout a kinetic run and at least 50% conversion to the chelator was observed spectrophotometrically. The negative slope of the linear fit of ln(Abs) at the λ_{max} characteristic of the prochelator *vs* time plot provided the observed rate constant k_{obs}. Equivalent values were obtained by using the increase in λ_{max} of the chelator. For each pro-chelator k_{obs} was determined at five different H_2O_2 concentrations. The slope of the linear fit of k_{obs} *vs* $[H_2O_2]$ provided k (M^{-1} s^{-1}).

2-Deoxyribose assay

The formation of hydroxyl radicals was measured by using a 2-deoxyribose oxidative degradation assay.[41] Because many standard buffers such as HEPES and TRIS are hydroxyl radical scavengers, all assays were performed in 50 mM NaH_2PO_4 buffered to pH 7.4. Standard reaction conditions consisted of 1 mL buffered solutions prepared by sequential addition of the following reagents at their final concentrations: 0–400 μM chelator or pro-chelator, 10 μM $FeCl_3$ or $CuSO_4$, 15 mM 2-deoxyribose, H_2O_2 (200 μM for iron assays and 100 μM for copper assays) and 2 mM ascorbic acid. The reactions were stirred for 60 min at 37 °C, then quenched with 1 mL of TBA and 1 mL of trichloroacetic acid. After heating to 100 °C for 20 min, the solutions were cooled to room temperature and the absorbance at 532 nm recorded. The data are reported as A/A_o, where A is the absorbance at a 532 nm at a specific chelator concentration, and A_o is the absorbance at 532 nm for the background reaction containing no added chelator. All measurements were performed in triplicate, and error bars reflect the standard deviation from triplicate runs.

Determination of partition coefficients

Solutions of 50–100 μM of compound were prepared in 50 mL of 1-octanol saturated with 50 mM aqueous phosphate buffered saline (PBS, pH = 7.4). The initial absorbance of this stock solution was measured to provide A_o. Preliminary experiments were conducted to verify that these absorbance values increased linearly with concentration. Aliquots of this solution (x = 1–5 mL) were diluted with 1-octanol saturated with PBS to give a total volume of 5 mL, which were combined in 50 mL tubes with 45 mL of PBS saturated with 1-octanol. The partition mixtures were allowed to equilibrate for 5 days before the absorbance of the 1-octanol layer was measured (A_{oct}). Using this partition volume ratio of 9 : 1 (45 mL PBS/5 mL 1-octanol), the partition coefficient P was calculated according to the following equation:[45]

$$P = \frac{[\text{octanol}]}{[\text{aqueous phase}]} = 9\frac{(45A_{oct})}{(A_o x - 5A_{oct})}$$

This equation may be rearranged in terms of x so that the partition coefficient may be obtained from the slope of the plot of

x versus A_{oct}/A_o:

$$x = \left(\frac{405}{P} + 5\right)\frac{A_{oct}}{A_0}$$

Note added in proof

A separate report of a boronic acid pro-chelator has recently appeared.[i,ii]

(i) Y. Wei and M. Guo, *Angew. Chem., Int. Ed.*, 2007, **46**, 4722–4725.

(ii) Y. Wei and M. Guo, *Angew. Chem., Int. Ed.*, 2007, **46**, 6948.

Acknowledgements

This work was supported by Duke University and the Parkinson's Disease Foundation.

References

1 B. Halliwell and J. M. C. Gutteridge, *Free Radicals in Biology and Medicine*, 3rd edn, Oxford University Press, New York, 1999.
2 B. Halliwell, *J. Neurochem.*, 2006, **97**, 1634–1658.
3 L. Zecca, M. B. H. Youdim, P. Riederer, J. R. Conner and R. R. Crichton, *Nat. Rev. Neurosci.*, 2004, **5**, 863–873.
4 K. J. Barnham, C. L. Masters and A. I. Bush, *Nat. Rev. Drug Discovery*, 2004, **3**, 205–214.
5 J. L. Pierre and M. Fontecave, *BioMetals*, 1999, **12**, 195–199.
6 M. Valko, H. Morris and M. T. D. Cronin, *Curr. Med. Chem.*, 2005, **12**, 1161–1208.
7 D. T. Dexter, F. R. Wells, A. J. Lees, F. Agid, Y. Agid, P. Jenner and C. D. Marsden, *J. Neurochem.*, 1989, **52**, 1830–1836.
8 E. Sofic, W. Paulus, K. Jellinger, P. Riederer and M. B. H. Youdim, *J. Neurochem.*, 1991, **56**, 978–982.
9 J. L. Dunaief, *Invest. Ophthalmol. Visual Sci.*, 2006, **47**, 4660–4664.
10 M. B. H. Youdim, G. Stephenson and D. Ben, Shachar, *Ann. N. Y. Acad. Sci.*, 2004, **1012**, 306–325.
11 D. R. Richardson, *Ann. N. Y. Acad. Sci.*, 2004, **1012**, 326–341.
12 D. Kaur, F. Yantiri, S. Rajagopalan, J. Kumar, J. Q. Mo, R. Boonplueang, V. Viswanath, R. Jacobs, L. Yang, M. F. Beal, D. DiMonte, I. Volitaskis, L. Ellerby, R. A. Cherny, A. I. Bush and J. K. Andersen, *Neuron*, 2003, **37**, 899–909.
13 D. Ben, Shachar, N. Kahana, V. Kampel, A. Warshawsky and M. B. H. Youdim, *Neuropharmacology*, 2004, **46**, 254–263.
14 Z. D. Liu and R. C. Hider, *Coord. Chem. Rev.*, 2002, **232**, 151–171.
15 A. Dedeoglu, K. Cormier, S. Payton, K. A. Tseitlin, J. N. Kremsky, L. Lai, X. H. Li, R. D. Moir, R. E. Tanzi, A. I. Bush, N. W. Kowall, J. T. Rogers and X. D. Huang, *Exp. Gerontol.*, 2004, **39**, 1641–1649.
16 A. Yiakouvaki, J. Savović, A. Al-Qenaei, J. Dowden and C. Pourzand, *J. Invest. Dermatol.*, 2006, **126**, 2287–2295.
17 A. Gaeta and R. C. Hider, *Br. J. Pharmacol.*, 2005, **146**, 1041–1059.
18 L. K. Charkoudian, D. M. Pham and K. J. Franz, *J. Am. Chem. Soc.*, 2006, **128**, 12424–12425.
19 M. Horackova, P. Ponka and Z. Byczko, *Cardiovasc. Res.*, 2000, **47**, 529–536.
20 D. R. Richardson and P. Ponka, *J. Lab. Clin. Med.*, 1998, **131**, 306–315.
21 T. Simunek, C. Boer, R. A. Bouwman, R. Vlasblom, A. M. G. Versteilen, M. Sterba, V. Gersl, R. Hrdina, P. Ponka, J. J. de Lange, W. J. Paulus and R. J. P. Musters, *J. Mol. Cell. Cardiol.*, 2005, **39**, 345–354.
22 H. G. Kuivila and A. G. Armour, *J. Am. Chem. Soc.*, 1957, **79**, 5659–5662.
23 L. C. Lo and C. Y. Chu, *Chem. Commun.*, 2003, 2728–2729.
24 A. E. Albers, V. S. Okreglak and C. J. Chang, *J. Am. Chem. Soc.*, 2006, **128**, 9640–9641.
25 M. C. Y. Chang, A. Pralle, E. Y. Isacoff and C. J. Chang, *J. Am. Chem. Soc.*, 2004, **126**, 15392–15393.
26 E. W. Miller, A. E. Albers, A. Pralle, E. Y. Isacoff and C. J. Chang, *J. Am. Chem. Soc.*, 2005, **127**, 16652–16659.
27 E. W. Miller, O. Tulyathan, E. Y. Isacoff and C. J. Chang, *Nat. Chem. Biol.*, 2007, **3**, 263–267.
28 W. Q. Yang, X. Gao, and B. H. Wang, in *Boronic Acids*, ed. D. G. Hall, Wiley-VCH, Weinheim, 2005, pp. 481-512.
29 D. S. Kalinowski and D. R. Richardson, *Pharmacol. Rev.*, 2005, **57**, 547–583.
30 A. A. Aruffo, T. B. Murphy, D. K. Johnson, N. J. Rose and V. Schomaker, *Acta Crystallogr., Sec. C*, 1984, **C40**, 1164–1169.
31 L. H. Huo, S. Gao, J. W. Liu, J. Li, H. Zhao and J. G. Zhao, *Acta Crystallogr., Sect. E*, 2004, **E60**, m673–m675.
32 T. B. Murphy, N. J. Rose, V. Schomaker and A. Aruffo, *Inorg. Chim. Acta*, 1985, **108**, 183–194.
33 A. Kapor, B. Ribar, V. M. Leovac, G. Argay, A. Kalman and S. Y. Chundak, *J. Coord. Chem.*, 1996, **38**, 139–144.
34 E. W. Ainscough, A. M. Brodie, A. J. Dobbs, J. D. Ranford and J. M. Waters, *Inorg. Chim. Acta*, 1998, **267**, 27–38.
35 S. C. Chan, L. L. Koh, P. H. Leung, J. D. Ranford and K. Y. Sim, *Inorg. Chim. Acta*, 1995, **236**, 101–108.
36 A.-M. Albrecth-Gary and A. L. Crumbliss, in *Metal Ions Biological Systems*, ed. A. Sigel and H. Sigel, Marcel Dekker, New York, 1973, vol. 35, pp. 239–327.
37 J. L. Buss, F. M. Torti and S. V. Torti, *Curr. Med. Chem.*, 2003, **10**, 1021–1034.
38 L. M. W. Vitolo, G. T. Hefter, B. W. Clare and J. Webb, *Inorg. Chim. Acta*, 1990, **170**, 171–176.
39 J. L. Buss and P. Ponka, *Biochim. Biophys. Acta*, 2003, **1619**, 177–186.
40 D. R. Richardson, L. M. W. Vitolo, G. T. Hefter, P. M. May, B. W. Clare, J. Webb and P. Wilairat, *Inorg. Chim. Acta*, 1990, **170**, 165–170.
41 B. Halliwell, J. M. C. Gutteridge and O. I. Aruoma, *Anal. Biochem.*, 1987, **165**, 215–219.
42 M. Hermes-Lima, M. S. Goncalves and R. G. Andrade, *Mol. Cell. Biochem.*, 2001, **228**, 73–82.
43 C. Hansch, *Acc. Chem. Res.*, 1969, **2**, 232–239.
44 J. T. Edward, F. L. Chubb and J. Sangster, *Can. J. Physiol. Pharmacol.*, 1997, **75**, 1362–1368.
45 P. V. Bernhardt, P. Chin, P. C. Sharpe, J. Y. C. Wang and D. R. Richardson, *J. Biol.Inorg. Chem.*, 2005, **10**, 761–777.
46 B. L. Rai, L. S. Dekhordi, H. Khodr, Y. Jin, Z. Liu and R. C. Hider, *J. Med. Chem.*, 1998, **41**, 3347–3359.
47 J. T. Edward, P. Ponka and D. R. Richardson, *Biometals*, 1995, **8**, 209–217.
48 J. T. Edward, *Biometals*, 1998, **11**, 203–205.
49 J. Yan, G. Springsteen, S. Deeter and B. H. Wang, *Tetrahedron*, 2004, **60**, 11205–11209.
50 J. T. Edward, M. Gauthier, F. L. Chubb and P. Ponka, *J. Chem. Eng. Data*, 1988, **33**, 538–540.
51 P. Ponka, J. Borova, J. Neuwirt and O. Fuchs, *FEBS Lett.*, 1979, **97**, 317–321.

